Alpine metamorphism in the central segment of the Western Greywacke Zone (Eastern Alps)

GERD RANTITSCH[1] and KATALIN JUDIK[2]

[1]Department of Applied Geosciences and Geophysics, University of Leoben, Peter Tunner Straße 5, A-8700 Leoben, Austria; gerd.rantitsch@unileoben.ac.at
[2]Institute for Geochemical Research, Hungarian Academy of Sciences, Budaörsi út. 45, H-1112 Budapest, Hungary; judik@geochem.hu

Abstract: The metamorphic pattern of the central Western Greywacke Zone (Austroalpine, Eastern Alps) was investigated by organic matter reflectance, Raman spectroscopy on organic matter and clay mineralogical methods. Raman data map a 10 km wide thermal aureole along the contact zone of the Greywacke Zone to the Penninic Tauern Window. The estimated maximum temperatures of 400 °C to 200 °C decrease from South to North, that is from the contact to the uppermost parts of the Greywacke Zone. This pattern is explained by an Oligocene to Miocene thermal pulse, related to the rapid exhumation of formerly deeply buried rocks of the Penninic unit. During this event, advective heat transport and circulating fluids overprinted the Cretaceous higher anchi- to lower epizonal metamorphic pattern of the central Western Greywacke Zone.

Key words: Eastern Alps, Greywacke Zone, Raman spectroscopy, organic matter, illite Kübler index.

Introduction

The orogenic evolution of the Eastern Alps was driven by two collisional events that occurred during Cretaceous and Paleogene times (Froitzheim et al. 1996; Genser et al. 1996). Both events were followed by orogen-parallel extension which resulted in the exhumation of deeper crustal rocks to higher crustal levels (e.g. Neubauer et al. 1995).

Subsequent to the early Late Cretaceous closing of the Meliata Ocean (e.g. Schmid et al. 2004), the newly formed Eoalpine nappe stack collapsed during Late Cretaceous to Paleogene times and formerly deeply buried metamorphic rocks of the Austroalpine units were exhumed (Neubauer et al. 1995; Bojar et al. 2001; Kurz & Fritz 2003; Tencer & Stüwe 2003; Robl et al. 2004; Wiesinger et al. 2006; Krenn et al. 2008). The reconstruction of the metamorphic pattern in this tectonic setting is hampered by the fact that metamorphic index minerals are very often missing. However, the hanging wall units of Late Cretaceous to Paleogene detachments are formed partly by metasediments containing a significant amount of organic matter. This enables the application of the "Raman spectroscopy of carbonaceous material" (RSCM) thermometer (Beyssac et al. 2002a,b) to separated organic materials (Rantitsch et al. 2004) as a simple technique to determine metamorphic gradients. Using this approach, Rantitsch et al. (2004, 2005) proposed that low- to very low-grade metamorphic hanging wall units at the eastern segment of the Eastern Alps (Graz Paleozoic and Eastern Greywacke Zone, see Fig. 1), tectonically overlying decompressed middle- to high-grade metamorphic rocks, were overprinted by advective heat and convective fluids during Late Cretaceous to Paleogene times.

By the Eocene collision of the European Plate with the Apulian Plate (e.g. Kurz et al. 1998, 2001; Kurz 2006), the Austroalpine tectonic units were thrusted over the Penninic nappes. During subsequent exhumation of the Penninic rocks, the Tauern Window (Fig. 1) was formed (e.g. Frisch et al. 2000).

This study focuses on the metamorphic imprint on a N-S-section across the Salzachtal-Ennstal-Mariazell-Puchberg (SEMP) Fault Zone, representing the northern margin of the Tauern Window (Fig. 1). The study area covers the central Western Greywacke Zone, an Austroalpine tectonic unit directly adjacent to the tectonically lower Penninic unit (Fig. 1). Because this unit is composed of metasediments, lacking metamorphic index minerals, the RSCM thermometer is used to estimate metamorphic peak temperatures. The reaction progress of organic and inorganic temperature indicators are different (e.g. Hillier et al. 1995; Sachsenhofer et al. 1998). Therefore, clay mineralogical data are discussed together with the RSCM data. The obtained data constrain the thermal effects during the exhumation stage of the Penninic units and demonstrate the significance of advective heat transport during late-stage orogenic processes within the Eastern Alps.

Geological setting

The studied section cuts the contact between the Penninic Tauern Window and the Austroalpine nappe pile, represented by the central Western Greywacke Zone and the Northern Calcareous Alps (Fig. 1). The exposed crustal section resulted from the subduction of the Penninic Ocean (e.g. Schmid et al. 2004) and the subsequent Eocene continent-continent-collision of the European lower plate with the Apulian upper plate (e.g. Kurz et al. 1998, 2001; Kurz 2006). The present contact between those units is represented by the SEMP Fault Zone (Ratschbacher et al. 1991; Linzer et al. 1997;
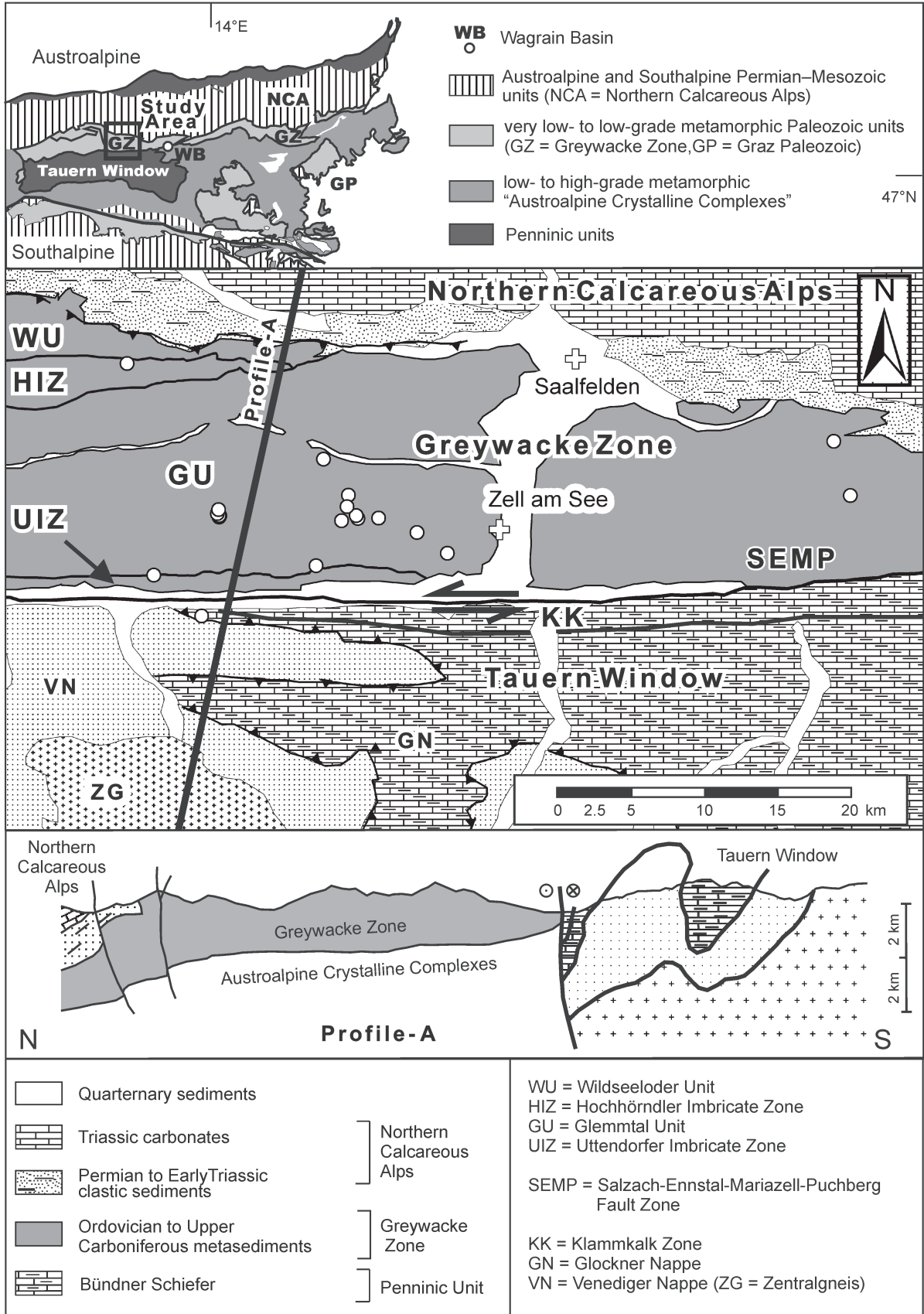
Fig. 1. Location of the study area and sample localities (white circles; for the coordinates see the Appendix) within the Eastern Alps (simplified geological map and section after Pestal et al. 2005 and Heinisch et al. 1995, 2003).

Wang & Neubauer 1998; Neubauer et al. 1999; Cole et al. 2007; Rosenberg & Schneider 2008), active since the Late Eocene/Oligocene (Urbanek et al. 2002) during exhumation of the Penninic Tauern Window in a sinistral wrench corridor (Ratschbacher et al. 1989; Peresson & Decker 1997; Reinecker & Lenhardt 1999; Frisch et al. 2000). This brittle to ductile (Cole et al. 2007; Rosenberg & Schneider 2008) fault zone separates the low-grade metamorphic (Hoinkes et al. 1999) rocks of the central Western Greywacke Zone from formerly deeply buried greenschist- to eclogite-grade metamorphic rocks of the Penninic Tauern Window. In a N-S section, $^{40}Ar/^{39}Ar$ age data from fine white mica fractions decrease from 113–120 Ma (Frank & Schlager 2006) in the Mesozoic cover of the Greywacke Zone (Northern Calcareous Alps) to 90–115 Ma in the Greywacke Zone (Urbanek et al. 2002) and 28–35 Ma at the northern margin of the Tauern Window (Urbanek et al. 2002). This indicates a dominant Cretaceous (Aptian to Cenomanian) tectono-metamorphic imprint of the Greywacke Zone (Frank & Schlager 2006) succeeded locally by a tectonothermal event, causing partial reset of the Ar geochronometer in latest Eocene to Oligocene times along the contact between the Greywacke Zone and the Penninic units in the Tauern Window.

In the study area, the Penninic unit comprises from bottom to top, the Venediger Nappe (a Subpenninic nappe according to Schmid et al. 2004), the Glockner Nappe (a Lower Penninic nappe according to Schmid et al. 2004) and the Klammkalk Zone (part of the Upper Penninic nappes according to Schmid et al. 2004). The Venediger Nappe is composed of crystalline rocks intruded by Variscan granitoids ("Zentralgneis") and partly covered by post-Variscan metasediments of Carboniferous to Cretaceous/Paleogene age (e.g. Frisch 1980). The Glockner Nappe and the Klammkalk Zone are composed mainly by calcareous schists ("Bündner Schiefer") of the former Penninic Ocean (e.g. Frisch 1980).

The polyphase metamorphic evolution of the central Penninic unit (e.g. Frank et al. 1987; Hoinkes et al. 1999; Kurz et al. 2001) resulted in a north-to-south increase (Frank et al. 1987) of the Eocene/Oligocene greenschist to amphibolite facies metamorphic overprint ("Tauern event"). In the Venediger Nappe peak temperatures are about 500–550 °C (e.g. Hoinkes et al. 1999; Schuster et al. 2004) at ca. 30 Ma, whereas cooling below 300 °C occurred at 25–30 Ma in the central part of the Venediger Nappe (Handy & Oberhänsli 2004). At the northern margin of the Tauern Window, the metamorphic peak reached lower- to upper greenschist facies (380 to 400 °C; Frank et al. 1987; Dingeldey et al. 1997; Bousquet et al. 2008), 28–35 Ma ($^{40}Ar/^{39}Ar$ fine white mica fractions age data from Urbanek 2001; see also Ratschbacher et al. 2004) ago. Subsequent cooling during Early to Late Miocene (23–13 Ma) extensional related exhumation (Ratschbacher et al. 1989; Frisch et al. 1998, 2000; Liu et al. 2001; Glodny et al. 2008) is recorded by fission track data (Grundmann & Morteani 1985; Staufenberg 1987; Dunkl et al. 2003). According to Kuhlemann et al. (2001), at 17 Ma the exhumation rate was accelerated for a short time interval (1 to 1.5 Myr) from 1.5–2 mm/yr to 5 mm/yr. During the Middle Miocene (14–10 Ma) the Penninic rocks were already exposed to the surface (Frisch et al. 2000).

The Western Greywacke Zone comprises Ordovician to Mississippian (Ebner et al. 2008) metasediments and basic volcanics (Heinisch et al. 1987) of several tectonic units (Wildseeloder Unit, Hochhörndler Imbricate Zone, Glemmtal Unit, Uttendorfer Imbricate Zone; Heinisch et al. 1995, 2003; Fig. 1). This sequence is overlain by Permian to Lower Triassic clastics and Triassic to Lower Cretaceous carbonates of the Tirolian Nappe System of the Northern Calcareous Alps (Fig. 1). In the Greywacke Zone, illite Kübler index data (Schramm 1980, 1982; Kralik et al. 1987; Kralik & Schramm 1994) indicate a Cretaceous (Kralik 1983; Kralik & Schramm 1994; Urbanek et al. 2002; Frank & Schlager 2006; Schmidlechner et al. 2006) epizonal metamorphic imprint. According to $^{40}Ar/^{39}Ar$ age data, synkinematically grown muscovite flakes record the metamorphic peak at 98 to 102 Ma and also give evidence for a second metamorphic event at ca. 70 Ma (Schmidlechner et al. 2006). The later event may be explained by an advective heating during exhumation of the underlying Austroalpine metamorphic complexes (Schmidlechner et al. 2006). In the vicinity of the SEMP Fault Zone, a rejuvenation of the Cretaceous $^{40}Ar/^{39}Ar$ age data to Early Oligocene (28–35 Ma) ages (Urbanek 2001; Urbanek et al. 2002) suggests a thermal overprint of the southern segment of the Greywacke Zone during exhumation of the underlying Penninic unit.

Samples and methods

The investigated section is covered in the Greywacke Zone by 22 samples of black slates, lydites and siltstones. One calcareous slate sample was taken in the Penninic unit (Fig. 1, Appendix). Only samples without microscopic evidence of oxidation were analysed.

On sections cut perpendicular to the foliation, the rank of organic maturation was determined by measurement of the maximum and minimum organic matter reflectance (Rmax, Rmin) under oil immersion in polarized light at a wavelength of 546 nm.

Samples were cleaned, crushed and disaggregated by slight grinding in an agate mortar for one minute. Because the Raman spectra of carbonaceous material (CM) are strongly affected by disorder due to friction, samples for Raman microspectrography are separated using a hydrochloric and hydrofluoric acid-treatment. Raman spectra were acquired by using a Dilor confocal Raman spectrometer equipped with a frequency-doubled Nd-YAG laser (100 mW, 532.2 nm) and diffraction gratings of 1200 and 1800 grooves/mm. Detection is with a Peltier-cooled, slow-scan, CCD matrix-detector. Laser focusing and sample viewing are performed through an Olympus BX 40 microscope fitted with a 50× long-working distance objective lens. To obtain a better signal to noise ratio five scans with an acquisition time of 30 sec in the 700–2000 cm^{-1} (first-order) and 2200–3200 cm^{-1} (second-order) region are summed to a composite spectra. On each sample, five composite spectra were recorded on different measurement spots. We focus on the first-order peaks at ~1350 cm^{-1} (D1 band), ~1580 cm^{-1} (G band), ~1610 cm^{-1} (D2 band), and ~1500 cm^{-1} (D3 band), and on the second-

order peaks at ~2700 cm^{-1} (S1 band), ~2400 cm^{-1} and ~2900 cm^{-1} (S2 band). Peak position, band area and band width (full width at half maximum, FWHM) of these peaks were determined using the computer program Labspec 2.08 (Dilor SA). Decomposition of the spectra was attained by fitting a combination of Gaussian and Lorentzian functions to the recorded data.

X-ray powder diffractometric (XRPD) patterns were obtained using a Philips PW-1730 diffractometer (with computerized APD system) with the following instrumental and measuring conditions: CuKα radiation, 45 kV/35 mA, proportional counter, graphite monochromator, divergence and detector slit of 1°, and collection of data with 0.01 and 0.02° 2Θ steps, using time intervals of 1 and 5 s, respectively. Diffraction patterns were performed from non-orientated and highly orientated powder mounts of whole rock and <2 μm spherical equivalent diameter (SED) size fraction samples in order to determine bulk-rock mineral assemblages, b cell dimension, and illite Kübler indices (KI, see Guggenheim et al. 2002). The <2 μm grain size fraction samples were obtained using the following procedure. Rock samples were disaggregated under standard conditions using a jaw crusher followed by crushing in a mortar mill for 3 min. Further disaggregating was achieved by repeated shaking in deionized water. The <2 μm grain size fraction was separated from aqueous suspension based on the differential settling of grains of different diameters. Following the technique of Kübler (1975), aqueous suspensions of 3 mg/cm^2 were mounted onto glass slides and dried at room temperature. Portions of air-dried <2 μm grain size fraction were saturated with ethylene glycol (60 °C overnight) in order to identify the possible swelling phases of the samples. The measured KI data are calibrated using the standards of the Kübler laboratory (for details see Árkai et al. 1995). The boundaries of the anchizone are defined by KI values of 0.25 and 0.42 Δ°2θ, respectively (Kübler 1967, 1968, 1990). The determination of the illite/K-white mica b dimension is a widely used method for the estimation of the pressure conditions of low- and very low-grade metamorphic alteration of fine-grained siliciclastic rocks (Sassi 1972; Sassi & Scolari 1974; Padan et al. 1982). Diffraction patterns were performed as described above from non-orientated powder mounts of whole rock samples with a mineralogical composition as recommended by Guidotti & Sassi (1976, 1986).

Results

XRPD indicates that the samples contain dominantly quartz, chlorite and illite/K-white mica, subordinately plagioclase, pyrite and rutile, as well as calcite and dolomite in variable proportions. No swelling clay mineral phases can be detected in the sample set. In two samples, paragonite is present (Table 1). The KI data of the examined samples (Table 1) generally fall into the high-temperature part of the anchizone (0.35 < IC [Δ°2θ] > 0.25) and into the epizone (KI < 0.25 Δ°2θ). Higher ranked (epizonal) samples are observed in the southern segment of the examined section (Fig. 2). The obtained b values (Table 1) mainly fall in the

medium-pressure zone or lie at the boundary between the low- and medium pressure zones of Guidotti & Sassi (1986).

Only two samples (20, 50) contain organic particles suitable for reflectance measurements. Organic matter reflectance of these samples (Table 2) indicates the Meta-Anthracite stage of the ASTM classification.

The Raman spectra (Table 3) reflect the continuous ordering of CM by a progressive thermal overprint (Fig. 3; Beyssac et al. 2002a,b). The calculated R2 peak area-ratio (D1/(G+D1+D2)) correlates inversely to the peak metamorphic temperature (Beyssac et al. 2002a,b). In low metamorphic conditions (R2 > 0.70), no variation of the peak positions and widths can be observed. With rising metamorphic rank (R2 < 0.70), the D1, D2, S1, and S2 peaks shift to higher, the G peak shifts to lower Raman values and the first-order FWHM values become narrower (Fig. 4). The regional pattern of the R2 ratios is presented in Fig. 5.

Discussion

The observed KI data do not trace a metamorphic gradient. This is explained by a lower sensitivity of this parameter compared to organic temperature indicators. However, if the

Table 1: Kübler Index (KI) in Δ°2θ (underlined samples contain paragonite) and K-white mica b dimension (Å) of the investigated samples.

Sample	KI	b
20	0.210	9.018
21	0.233	9.016
23	0.227	9.013
24	0.280	9.008
25	0.274	8.993
26	0.239	8.999
27	0.226	9.018
30	0.221	9.011
32	0.239	-
33	0.218	9.002
34	0.242	9.005
35	0.249	8.995
36	-	9.001
37	0.249	8.999
37a	0.246	9.006
40	0.240	9.019
41	0.250	9.002
42	0.221	9.043
43	0.239	-
44	0.250	-
45	-	9.006
46	0.265	-
47	0.236	-
50	0.287	-

Table 2: Vitrinite reflectance (R$_{max}$, R$_{min}$) in two samples of the central Western Greywacke Zone (sd = standard deviation, N = number of measurements).

Sample	R$_{max}$	sd	N	R$_{min}$	sd	N
20	7.55	0.63	5	2.69	0.31	3
50	7.96	0.39	18	2.39	0.33	18

Table 3: Mean values and standard deviation (sd) of the parameters (position, width = full width at half maximum) obtained from the decomposition of 5 Raman spectra per sample. Peak metamorphic temperatures (Temp) were calculated after Rahl et al. (2005).

ID	D1				D3				G				D2				S1				S2				R1		R2		Temp	
	position	sd	width	sd	position	sdv	width	sd	position	sd	width	sd	position	sd	width	sd	position	sd	width	sd	position	sd	width	sd	mean	sd	mean	sd	mean	+/-
44	1354.8	1.5	53.5	4.9					1586.9	1.0	31.6	1.5	1625.5	1.7	17.3	4.8	2702.3	1.7	77.1	3.1	2943.0	3.8	89.0	22.6	0.62	0.06	0.48	0.03	389	19
42	1350.8	1.4	41.2	2.0					1583.8	1.7	27.8	2.3	1621.8	1.8	19.3	2.2	2698.4	3.5	67.0	3.5	2940.8	2.9	72.9	4.6	0.78	0.08	0.50	0.01	402	5
43	1352.3	0.5	41.1	2.4					1586.0	0.2	31.4	2.1	1622.7	1.5	20.1	2.9	2701.1	0.2	52.1	2.8	2946.0	3.9	82.3	18.6	0.89	0.04	0.51	0.03	418	22
46	1355.8	1.2	44.7	1.2	1513.7	5.5	92.6	17.8	1588.5	1.3	28.9	1.1	1625.5	1.1	16.2	0.3	2702.3	1.5	75.0	3.5	2945.8	1.8	83.1	4.0	0.84	0.09	0.52	0.03	397	17
30	1354.0	0.7	44.4	2.6	1542.7	15.9	204.7	39.4	1589.1	0.4	35.8	3.7	1624.3	1.1	22.0	3.9	2699.7	2.4	64.6	8.3	2944.9	1.3	65.6	9.5	1.32	0.07	0.58	0.02	406	10
26	1350.2	0.3	51.4	2.6	1553.3	11.8	100.5	8.2	1590.1	1.6	41.3	5.8	1619.9	1.7	27.1	1.0	2694.3	0.6	79.9	7.4	2941.4	2.5	113.5	13.8	1.80	0.15	0.63	0.03	381	33
21	1350.2	0.8	53.4	2.5	1548.3	15.0	104.9	16.1	1594.4	2.7	43.6	3.1	1620.4	1.4	26.2	2.8	2694.2	1.3	96.3	6.6	2938.0	2.5	87.5	8.5	1.96	0.15	0.66	0.01	354	14
45	1353.9	0.3	48.8	2.3	1525.1	10.7	105.8	24.1	1595.5	0.7	43.4	1.4	1625.1	0.5	23.5	2.1	2696.7	0.3	76.8	1.6	2943.0	0.6	80.6	2.1	2.10	0.10	0.66	0.02	352	21
37A	1354.6	0.9	56.2	0.9	1548.6	17.9	134.7	42.0	1595.1	4.7	39.8	2.7	1623.8	3.0	29.4	2.0	2699.0	3.1	93.7	7.5	2942.1	3.2	108.0	12.0	1.85	0.34	0.66	0.05	346	50
33	1351.6	0.3	56.1	2.1	1544.9	6.9	118.9	3.5	1596.1	1.2	43.1	2.5	1622.6	0.7	27.3	2.0	2695.6	0.5	102.7	4.4	2939.2	1.0	120.0	4.0	1.97	0.12	0.68	0.01	333	16
27	1353.7	0.1	48.5	1.1	1554.5	8.4	95.7	17.1	1594.2	1.8	35.0	1.5	1625.4	0.7	26.1	1.5	2697.2	1.1	77.2	3.4	2944.0	0.6	85.7	9.5	2.05	0.24	0.68	0.03	330	40
34	1350.4	0.3	51.9	2.8	1557.8	11.7	99.1	14.0	1591.2	1.1	35.7	3.7	1620.5	1.2	27.7	2.0	2695.7	0.7	86.5	7.5	2940.1	1.0	93.4	20.1	2.02	0.18	0.68	0.03	330	32
36	1351.2	0.9	57.9	1.8	1540.3	4.4	124.5	16.2	1595.4	1.4	44.3	1.4	1621.7	1.4	28.3	2.4	2695.5	1.3	101.1	7.0	2938.7	2.8	120.6	10.8	2.00	0.10	0.68	0.01	328	12
35	1349.3	0.5	55.4	2.1	1543.3	2.8	115.9	5.5	1593.1	0.9	42.7	0.9	1620.6	0.9	26.4	1.6	2691.6	2.5	90.8	10.7	2940.6	2.1	87.4	20.6	2.09	0.07	0.69	0.01	324	12
32	1349.8	0.3	61.2	3.7	1546.8	20.8	107.1	14.7	1594.8	4.0	42.7	4.0	1620.5	1.9	26.3	6.2	2693.2	2.0	91.6	14.8	2940.6	1.9	88.8	19.3	1.86	0.16	0.69	0.05	320	47
23	1350.6	0.3	50.0	1.6	1553.2	5.9	105.5	37.4	1595.5	1.3	39.2	2.5	1622.0	0.9	25.2	2.5	2693.1	0.9	87.3	3.5	2939.8	0.8	91.2	4.6	2.29	0.18	0.70	0.02	306	32
25	1347.7	1.3	52.7	5.0	1555.9	4.1	100.8	5.1	1589.9	0.6	36.8	1.7	1619.4	1.1	26.2	1.1	2690.6	2.1	93.6	11.6	2935.7	3.3	115.1	16.4	2.07	0.13	0.70	0.02	309	21
20	1345.0	1.2	57.1	1.4	1544.0	10.5	115.1	5.2	1587.7	1.3	42.1	1.3	1615.9	1.3	29.1	1.0	2686.4	2.2	97.1	8.2	2930.3	3.6	106.5	8.6	2.19	0.07	0.71	0.02	299	20
24	1350.1	0.8	86.9	5.7	1561.1	4.3	111.8	6.7	1606.9	1.2	43.1	0.6					2694.1	3.1	175.4	9.6	2935.3	2.5	176.0	3.9	1.22	0.05	0.73	0.02	227	14
37	1348.8	0.4	59.3	2.2	1555.6	10.7	132.4	11.2	1602.6	1.3	44.4	1.7					2687.7	4.9	139.3	35.3	2939.8	3.2	77.0	18.7	1.86	0.15	0.74	0.03	264	28
41	1349.6	1.1	70.2	8.8	1554.7	3.4	125.8	7.6	1605.4	1.4	42.4	1.2					2684.6	3.7	180.9	28.1	2938.6	2.8	126.4	11.7	1.61	0.09	0.75	0.02	242	16
HF	1343.5	0.9	108.3	5.7	1540.4	2.7	144.0	3.3	1601.8	1.9	46.5	1.0					2690.5	7.5	312.7	19.9	2935.8	1.0	174.6	4.7	1.29	0.07	0.76	0.02	208	9
40	1345.5	2.0	81.9	3.6	1543.8	12.2	135.5	13.1	1596.7	4.9	48.6	3.1					2680.2	1.5	202.2	48.2	2931.6	4.3	130.5	16.7	1.71	0.18	0.77	0.03	233	23

major KI zones are mapped (Fig. 2), a south-to-north decrease of the metamorphic overprint can be detected from the data. Most of the samples do not contain CM large enough for reliable reflectance measurements. Therefore, organic matter reflectance is also not suitable for a detailed mapping of the metamorphic pattern. However, Figure 5 demonstrates that RSCM is able to reconstruct a metamorphic field gradient in the study area.

Rantitsch et al. (2004) modified the temperature calibration of Beyssac et al. (2002b), being valid in the temperature range between 330 and 650 °C. On the basis of low-temperature thermo-chronological data, Rahl et al. (2005) extended the calibration range to temperatures down to 100 °C. To relate the observed high R2 ratios consistently to metamorphic temperatures, the calibration of Rahl et al. (2005) is used in this study (Table 3). This results in the reconstruction of a temperature gradient of 400 °C to 200 °C, decreasing from the SEMP Fault Zone towards the base of the Northern Calcareous Alps (Fig. 5). It is important to note that there is no break in the peak metamorphic temperature across the boundary between the Penninic unit and the Greywacke Zone. The internal faults of the Greywacke Zone also do not disturb the temperature pattern. There is no correlation between the Raman parameter and the altitude of the sample locality. Due to the regional geological setting, we exclude therefore a trend of rising metamorphic temperatures into deeper structural levels. Up to a distance of ca. 10 km from the SEMP Fault Zone, the trend is exposed continuously. Further to the North the RSCM thermometer suggests a more homogeneous pattern.

The estimated temperature of the sample from the Penninic unit is in good accordance with the estimate from the calcite-dolomite geothermometry of Frank et al. (1987) and supports therefore the reliability of the RSCM thermometer (Beyssac et al. 2002a,b; Rantitsch et al. 2004; Rahl et al. 2005) in rock sequences lacking pressure-temperature-critical mineral assemblages. The comparison between the Raman and KI data demonstrates a higher sensitivity of the organic parameter in contrast to the inorganic parameter in very low- to low-grade metasediments.
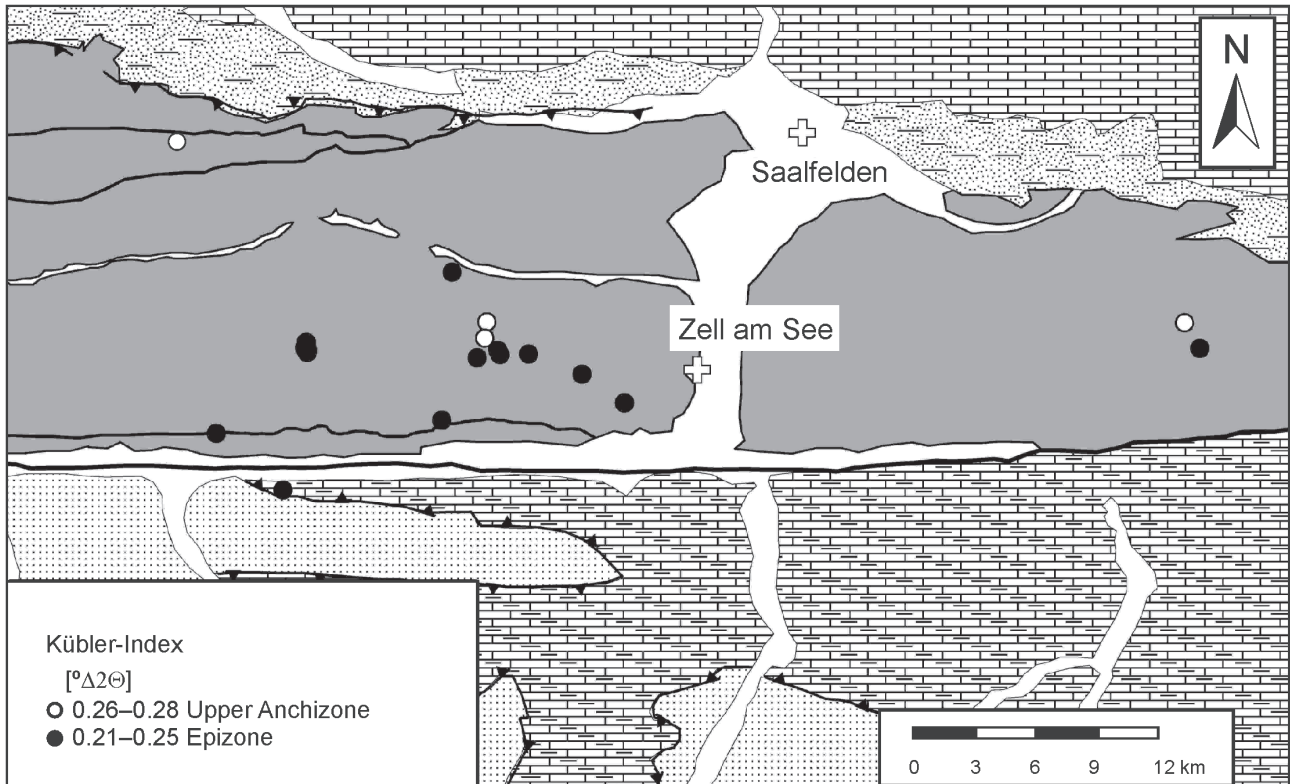
Fig. 2. Distribution of illite Kübler-indices (KI) in the study area (Legend see Fig. 1).

The described metamorphic pattern can be explained by the thermal influence of the rising Penninic unit on the overlying Greywacke Zone. This hypothesis is supported by the age data of Urbanek (2001). Further evidence is given by the regional paleo-heat flow pattern within Miocene sedimentary basins, formed as pull-apart basins during the Early- to Mid-

dle Miocene uplift of the Penninic unit (Sachsenhofer 1992, 2001). The data suggest that in the area above the rising Penninic unit, the heat flow extremely increased to >200 mW/m^2 (Sachsenhofer 2001). Over greater distances, the heat flow decreased circularly (Sachsenhofer 2001). The central part of this heat flow anomaly covers the Wagrain Basin (Fig. 1), subsiding directly above the central Western Greywacke Zone. Consequently, we see in the study area evidence for a high heat flow during Early- to Middle Miocene times. Subsequently, during the Late Miocene, the heat flow decreased to 75 mW/m^2 (Fügenschuh 1995).

In the area of the Early- to Middle Miocene heat flow maximum, the estimated peak metamorphic temperature in the hanging wall unit (southern margin of the central Western Greywacke Zone) corresponds to the Eocene/ Oligocene metamorphic temperature maximum in the footwall unit (northern segment of the Penninic unit). Therefore, we suppose an isothermal decompression of the Penninic unit between 30 and 15 Ma (see also Dachs 1990; Neubauer et al. 1999), giving rise to a thermal overprint of the overlying Greywacke Zone. This is in accordance to geochronological data, indicating a cooling of the Penninic rocks below 400 °C in the time interval between 24 and 15 Ma (24–17 in the East, 17–15 in the West; Dunkl et al. 2003).
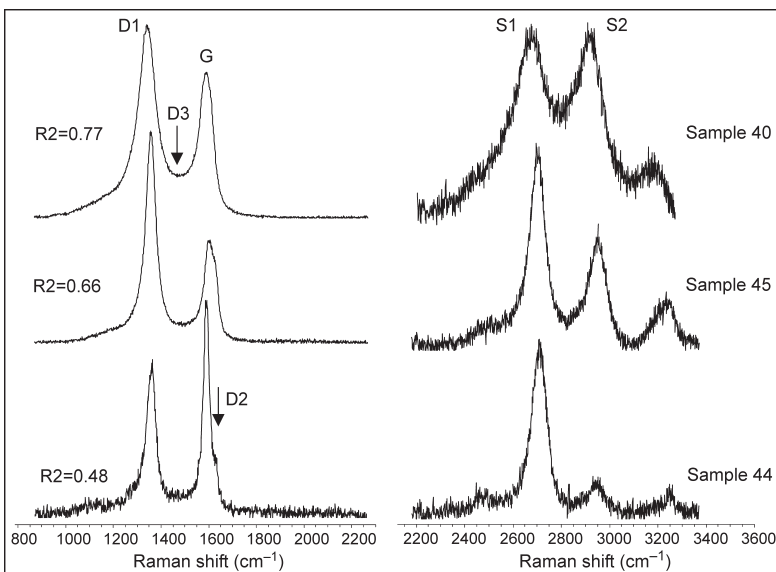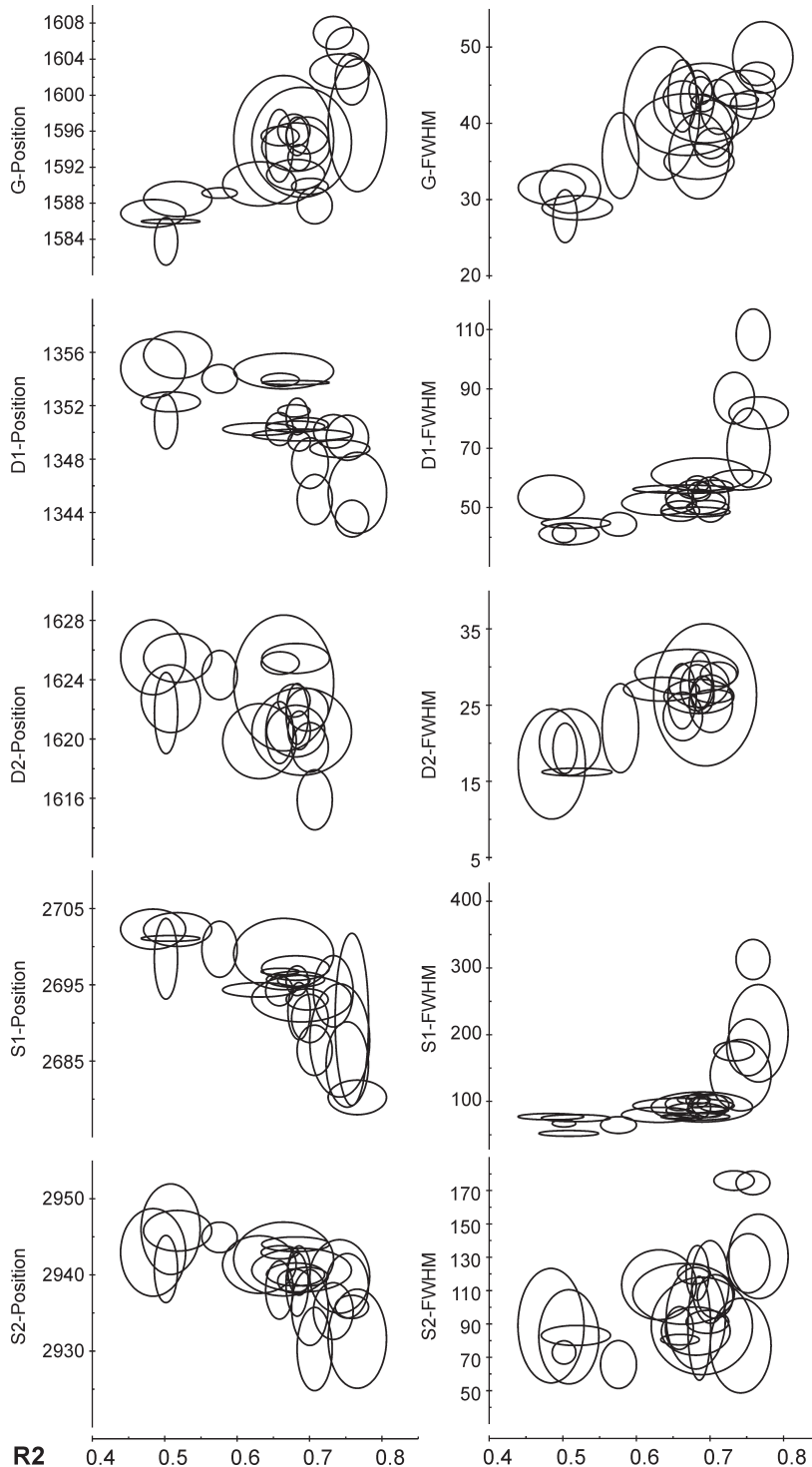

Fig. 3. Representative examples for first- and corresponding second-order Raman spectra (R2 is the R2 peak area ratio [D1/(G+D1+D2)]). The R2 values indicate a temperature rise from top to bottom.

Fig. 4. Relationship between the Raman peak parameter and the R2 peak area ratio [D1/(G+D1+D2)]; the centre of the ellipses plot the mean values, and the half-axes correspond to 2 standard deviations of the repeated measurements. Decreasing R2 values indicate rising metamorphic temperatures.
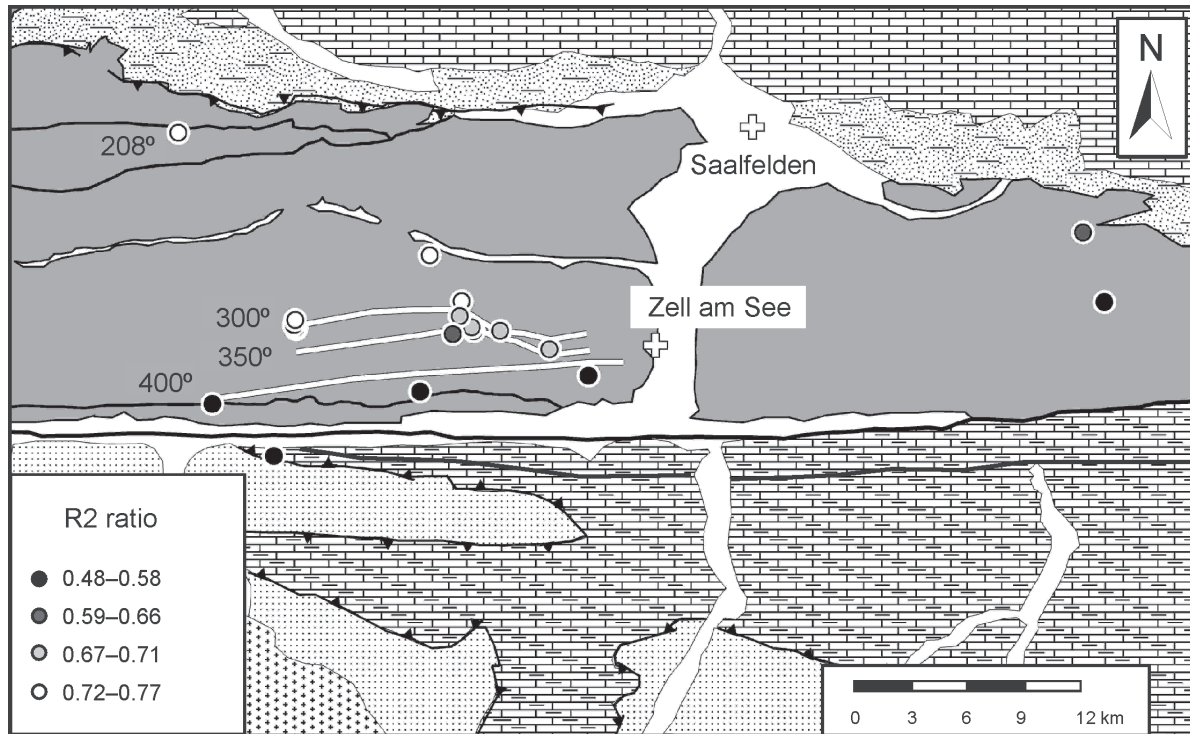
indicates that 400 °C, the temperature determined for the Oligocene to Miocene overprint, may have been too low to cause Ar resetting in the interior parts of the Greywacke Zone. The Ar-isotopic system in white mica closes in a temperature interval between ca. 350° (e.g. Dallmeyer & Takasu 1992; Lips et al. 1998) and ca. 500 °C (Hames & Cheney 1997), and other factors like ductile deformation or fluid flow may control the resetting (e.g. Villa 1998; Balogh & Dunkl 2005; Kurz et al. 2008). This fact explains a reset of $^{40}Ar/^{39}Ar$ white mica ages at the SEMP Fault Zone and a missing overprint of $^{40}Ar/^{39}Ar$ age spectra within the area of the observed thermal aureole.

If the intermediate pressure character of the obtained K-white mica b dimensions is taken into account, it may be supposed that the KI values record Cretaceous thrusting rather than the Miocene thermal overprint. If the clay mineralogical reactions were triggered by the later event, b dimensions should resemble the low pressure values (<9.000 Å) commonly found in extensional basins (Robinson & Bevins 1986; Merriman & Peacor 1999). Thus, if this supposition is correct, the data give evidence for a decoupling of inorganic and organic metamorphic processes.

The detected Early- to Middle Miocene thermal aureole on the southern margin of the central Western Greywacke Zone resembles in its structural setting the Late Cretaceous aureole within the eastern segment of the Greywacke Zone (Rantitsch et al. 2004). Similarly to the Late Cretaceous anomaly (Rantitsch et al. 2004), the Early- to Middle Miocene anomaly may have been accompanied by a convective heat loss due to fluid circulation (Neubauer et al. 1999), which resulted in a structurally controlled gold mineralization in the Penninic unit (Neubauer 2002; Putz et al. 2003).

Conclusions

Up to a distance of ca. 10 km from the SEMP Fault Zone, the Cretaceous high-temperature anchizonal to epizonal metamorphic pattern of the central Western Greywacke Zone is overprinted by a thermal aureole. The temperature influence diminishes from the South towards the North, that is from the contact with the Penninic rocks to the internal segments of the Greywacke Zone. By applying

Some unpublished Cretaceous $^{40}Ar/^{39}Ar$ white mica ages without evidence for a later thermal overprint have been reported from the southern segment of the Western Greywacke Zone (W. Frank and F. Neubauer, pers. comm. 2008). This

Fig. 5. Raman R2-ratio (Beyssac et al. 2002b) in the study area (Legend see Fig. 1). Isolines contour the temperature zonation according to the RSCM calibration of Rahl et al. (2005).

the "Raman spectroscopy of carbonaceous material" thermometer, the organic metamorphic pattern can be explained by a temperature gradient of 400 °C to 200 °C. This pattern is explained by an Oligocene to Miocene thermal pulse, related to the rapid exhumation of formerly deeply buried rocks of the Penninic unit. During this event, advective heat transport and circulating fluids overprinted the Cretaceous high-temperature anchi- to lower epizonal metamorphic pattern of the central Western Greywacke Zone.

References

Árkai P., Sassi F.P. & Sassi R. 1995: Simultaneous measurements of chlorite and illite crystallinity: a more reliable tool for monitoring low- to very low-grade metamorphism in metapelites. A case study from the Southern Alps (NE Italy). *European J. Mineralogy* 7, 1115–1128.

Balogh K. & Dunkl I. 2005: Argon and fission track dating of Alpine metamorphism and basement exhumation in the Sopron Mts. (Eastern Alps, Hungary): Thermochronology or mineral growth? *Miner. Petrology* 83, 191–218.

Beyssac O., Rouzaud J.N., Goffé B., Brunet F. & Chopin C. 2002a: Graphitization in a high-pressure, low-temperature metamorphic gradient: a Raman microspectroscopy and HRTEM study. *Contr. Mineral. Petrology* 143, 19–31.

Beyssac O., Goffé B., Chopin C. & Rouzaud J.N. 2002b: Raman spectra of carbonaceous material in metasediments: a new geothermometer. *J. Metamorph. Geology* 20, 859–871.

Bojar H.-P., Bojar A.-V., Mogessie A., Fritz H. & Thalhammer O.A.R. 2001: Evolution of veins and sub-economic ore at Strassegg, Paleozoic of Graz, Eastern Alps, Austria: evidence

for local fluid transport during metamorphism. *Chem. Geol.* 175, 757–777.

Bousquet R., Oberhansli R., Goffe B., Wiederkehr M., Koller F., Schmid S.M., Schuster R., Engi M., Berger A. & Martinotti G. 2008: Metamorphism of metasediments at the scale of an orogen: a key to the Tertiary geodynamic evolution of the Alps. *Geol. Soc. London, Spec. Publ.* 298, 393–411.

Cole J., Hacker B.R., Ratschbacher L., Dolan J., Seward G., Frost E. & Frank W. 2007: Fault-zone deformation and strain partitioning at the brittle-ductile transition: Example from the SEMP fault, Austrian Alps. *J. Geophys. Res., Solid Earth* 112, B12304.

Dachs E. 1990: Geothermobarometry in metasediments of the southern Grossvenediger area (Tauern Window, Austria). *J. Metamorph. Geology* 8, 217–230.

Dallmeyer R.D. & Takasu A. 1992: ^{40}Ar/^{39}Ar ages of detrital muscovite and whole-rock slate/phyllite, Narragansett Basin, RI-MA, USA: implications for rejuvenation during very low-grade metamorphism. *Contr. Mineral. Petrology* 110, 515–527.

Dingeldey Ch., Dallmeyer R.D., Koller F. & Massonne H.-J. 1997: P-T-t history of the Lower Austroalpine nappe complex in the Tarntaler Berge NW of the Tauern Window: implications for

the geotectonic evolution of the central Eastern Alps. *Contr. Mineral. Petrology* 129, 1–19.

Dunkl I., Frisch W. & Grundmann G. 2003: Zircon fission track thermochronology of the southeastern part of the Tauern Window and the adjacent Austroalpine margin. *Eclogae Geol. Helv.* 96, 209–217.

Ebner F., Vozárová A., Kovács S., Kräutner H.-G., Krstić B., Szederkényi T., Jamičić D., Balen D., Belak M. & Trajanova M. 2008: Devonian–Carboniferous pre-flysch and flysch environments in the Circum Pannonian Region. *Geol. Carpathica* 59, 2, 159–195.

Frank W. & Schlager W. 2006: Jurassic strike slip versus subduction in the Eastern Alps. *Int. J. Earth Sci.* 95, 431–450.

Frank W., Höck V. & Miller Ch. 1987: Metamorphic and tectonic history of the Central Tauern Window. In: Flügel H. & Faupl P. (Eds.): Geodynamics of the Eastern Alps. *Deuticke*, Wien, 34–54.

Frisch W. 1980: Post-Hercynian formations of the western Tauern window: sedimentological features, depositional environment, and age. *Mitt. Österr. Geol. Gesell.* 71/72, 49–63.

Frisch W., Kuhlemann J., Dunkl I. & Brügel A. 1998: Palinspastic reconstruction and topographic evolution of the Eastern Alps during late Tertiary tectonic extrusion. *Tectonophysics* 297, 1–15.

Frisch W., Dunkl I. & Kuhlemann J. 2000: Postcollisional orogen-parallel large-scale extension in the Eastern Alps. *Tectonophysics* 327, 239–265.

Froitzheim N., Schmid S.M. & Frey M. 1996: Mesozoic paleogeography and the timing of eclogite facies metamorphism in the Alps: A working hypothesis. *Eclogae Geol. Helv.* 89, 81–110.

Fügenschuh B. 1995: Thermal and kinematic history of the Brenner area (Eastern Alps, Tyrol). *Dr. Thesis, ETH Zürich*, 1–226.

Genser J., Van Wees J.D., Cloetingh S. & Neubauer F. 1996: Eastern Alpine tectono-metamorphic evolution: Constraints from two-dimensional P-T-t modeling. *Tectonics* 15, 584–604.

Glodny J., Ring U. & Kühn A. 2008: Coeval high-pressure metamorphism, thrusting, strike-slip, and extensional shearing in the Tauern Window, Eastern Alps. *Tectonics* 27, TC 4004.

Grundmann G. & Morteani G. 1985: The young uplift and thermal history of the central Eastern Alps (Austria/Italy), evidence from apatite fission track ages. *Jb. Geol. Bundesanst.* 128, 197–216.

Guggenheim S., Bain D.C., Bergaya F., Brigatti M.F., Drits V.A., Eberl D.D., Formoso M.L.L., Galan E., Merriman R.J., Peacor D.R., Stanjek H. & Watanabe T. 2002: Report of the Association Internationale por l'Etude des Argiles (AIPEA) Nomenclature Committee for 2001: Order, disorder, and crystallinity in phyllosilicates and the use of the "crystallinity index". *Clays and Clay Miner.* 50, 3, 406–409.

Guidotti C.V. & Sassi F.P. 1976: Muscovite as a petrogenetic indicator mineral in pelitic schists. *Neu. Jb. Mineral. Abh.* 127, 97–142.

Guidotti C.V. & Sassi F.P. 1986: Classification and correlation of metamorphic facies series by means of muscovite b0 data from low-grade metapelites. *Neu. Jb. Mineral. Abh.* 153, 363–380.

Hames W.E. & Cheney J.T. 1997: On the loss of ^{40}Ar from muscovite during polymetamorphism. *Geochim. Cosmochim. Acta* 61, 3863–3872.

Handy M.R. & Oberhänsli R. 2004: Explanatory notes to the map: Metamorphic structure of the Alps — Metamorphic structure of the Alps — Age map of the metamorphic structure of the Alps — tectonic interpretation and outstanding problems. *Mitt. Österr. Mineral. Gesell.* 149, 201–225.

Heinisch H., Sprenger W. & Weddige K. 1987: Neue Daten zur Altersstellung der Wildschönauer Schiefer und des Basaltvulkanismus im ostalpinen Paläozoikum der Kitzbühler Grauwackenzone (Österreich). *Jb. Geol. Bundesanst.* 130, 163–173.

Heinisch H., Pestal G., Stingl V. & Hellerschmidt-Alber J. 1995: Geologische Karte der Republik Österreich. Blatt 123 Zell am See. *Geol. Bundesanst.*, Wien.

Heinisch H., Pestal G., Reitner J. & Stingl V. 2003: Geologische Karte der Republik Österreich. Blatt 122 Kitzbühel. *Geol. Bundesanst.*, Wien.

Hillier S., Matyas J., Matter A. & Vasseur G. 1995: Illite/smectite diagenesis and its variable correlation with vitrinite reflectance in the Pannonian Basin. *Clays and Clay Miner.* 43, 174–183.

Hoinkes G., Koller F., Rantitsch G., Dachs E., Höck V., Neubauer F. & Schuster R. 1999: Alpine metamorphism of the Eastern Alps. *Schweiz. Mineral. Petrogr. Mitt.* 79, 155–181.

Kralik M. 1983: Interpretation of K-Ar and Rb-Sr data from fine fractions of weakly metamorphosed shales and carbonate rocks at the base of the Northern Calcareous Alps (Salzburg, Austria). *Tschermaks Mineral. Petrogr. Mitt.* 32, 49–67.

Kralik M. & Schramm J.-M. 1994: Illit-Wachstum: Übergang Diagenese-Metamorphose im Karbonat- und Tongesteinen der nördlichen Kalkalpen: Mineralogie und Isotopengeologie (Rb-Sr, K-Ar und C-O). *Jb. Geol. Bundesanst.* 137, 105–137.

Kralik M., Krumm H. & Schramm J.-M. 1987: Low grade and very low grade metamorphism in the Northern Calcareous Alps and in the Greywacke Zone: illite-crystallinity data and isotopic ages. In: Flügel H.W. & Faupl P. (Eds.): Geodynamics of the Eastern Alps. *Deuticke*, Wien, 164–178.

Krenn K., Fritz H., Mogessie A. & Schaflechner J. 2008: Late Cretaceous exhumation history of an extensional extruding wedge (Graz Paleozoic Nappe Complex, Austria). *Int. J. Earth Sci.* 97, 1331–1352.

Kuhlemann J., Frisch W., Dunkl I. & Székely B. 2001: Quantifying tectonic versus erosive denudation. The Miocene core complexes of the Alps. *Tectonophysics* 330, 1–23.

Kurz W. 2006: Penninic paleogeography from the Western towards the Eastern Alps — still open questions? *Int. Geol. Rev.* 48, 996–1022.

Kurz W. & Fritz H. 2003: Tectonometamorphic evolution of the Austroalpine Nappe Complex in the central Eastern Alps — consequences for the Eo-Alpine evolution of the Eastern Alps. *Int. Geol. Rev.* 45, 1100–1127.

Kurz W., Neubauer F., Genser J. & Dachs E. 1998: Alpine geodynamic evolution of passive and active continental margin sequences in the Tauern Window (Eastern Alps, Austria, Italy): a review. *Geol. Rdsch.* 87, 225–242.

Kurz W., Neubauer F., Genser J., Unzog W. & Dachs E. 2001: Tectonic evolution of Penninic units in the Tauern Window during the Paleogene: constraints from structural and metamorphic geology. In: Piller W.E. & Rasser M.W. (Eds.): Paleogene of the Eastern Alps. *Österr. Akad. Wissenschaften, Schriftenreihe Erdwissenschaftlichen Kommission* 14, 347–375.

Kurz W., Handler R. & Bertoldi Ch. 2008: Tracing the exhumation of the Eclogite Zone (Tauern Window, Eastern Alps) by ^{40}Ar/^{39}Ar dating of white mica in eclogites. *Swiss J. Geosci.* 101, Suppl. 1, 191–206.

Kübler B. 1967: La cristallinité de l'illite et les zones tout a fait superieures du métamorphisme. In: Etages Tectoniques, Colloque de Neuchâtel. *Université Neuchâtel*, 105–121.

Kübler B. 1968: Evaluation quantitative du métamorphisme par la cristallinité de l'illite. *Bull. Centre Recherche Pau-SNPA* 2, 385–397.

Kübler B. 1975: Diagenese-anchimétamorphisme et métamorphisme. *Inst. Nat. Res. Sci.-Pétrole*, Quebec.

Kübler B. 1990: Clay minerals, from deposition to metamorphism. Fine sediment mineralogical associations from diagenesis to metamorphism. *Mineral. Petrogr. Acta* 33, 15–27.

Linzer H.-G., Moser F., Nemes F., Ratschbacher L. & Sperner B. 1997: Build-up and dismembering of the eastern Northern Calcareous Alps. *Tectonophysics* 272, 97–124.

Lips A.L.W., White S.H. & Wijbrans J.R. 1998: $^{40}Ar/^{39}Ar$ laser-probe direct dating of discrete deformational events: a continous record of early Alpine tectonics in the Pelagonian Zone, NE Aegean area, Greece. *Tectonophysics* 298, 133–153.

Liu Y., Genser J., Handler R., Friedl G. & Neubauer F. 2001: $^{40}Ar/^{39}Ar$ muscovite ages from the Penninic-Austroalpine plate boundary, Eastern Alps. *Tectonics* 20, 526–547.

Merriman R.J. & Peacor D.R. 1999: Very low-grade metapelites: mineralogy, microfabrics and measuring reaction progress. In: Frey M. & Robinson D. (Eds.): Low-grade metamorphism. *Blackwell*, Oxford, 10–60.

Neubauer F. 2002: Contrasting Late Cretaceous with Neogene ore provinces in the Alpine-Balkan-Carpathian-Dinaride collision belt. In: Blundell D.J., Neubauer F. & von Quadt A. (Eds.): The timing and location of major ore deposits in an evolving orogen. *Geol. Soc. London, Spec. Publ.* 204, 81–102.

Neubauer F., Dallmeyer R.D., Dunkl I. & Schirnik D. 1995: Late Cretaceous exhumation of the metamorphic Gleinalm dome, Eastern Alps: kinematics, cooling history and sedimentary response in a sinistral wrench corridor. *Tectonophysics* 242, 79–89.

Neubauer F., Genser J., Kurz W. & Wang X. 1999: Exhumation of the Tauern Window, Eastern Alps. *Physics and Chemistry of the Earth, Part A: Solid Earth and Geodesy* 24, 675–680.

Padan A., Kisch H.J. & Shagam R. 1982: Use of the lattice parameter b0 of dioctahedral illite/muscovite for the characterization of P/T gradients of incipient metamorphism. *Contr. Mineral. Petrology* 79, 85–95.

Peresson H. & Decker K. 1997: The Tertiary dynamics of the northern Eastern Alps (Austria): Changing palaeostresses in a collisional plate boundary. *Tectonophysics* 272, 125–157.

Pestal G., Hejl E., Egger H., van Husen D., Linner M., Mandl G.W., Moser M., Reitner J., Rupp Ch. & Schuster R. 2005: Geologische Karte von Salzburg 1:200,000. *Geol. Bundesanst.*, Wien.

Putz H., Paar W.H., Topa D., Horner J. & Lüders V. 2003: Structurally controlled gold and sulfosalt mineralization: The Altenberg example, Salzburg Province, Austria. *Miner. Petrology* 78, 111–138.

Rahl J.M., Anderson K.M., Brandon M.T. & Fassoulas C. 2005: Raman spectroscopic carbonaceous material thermometry of low-grade metamorphic rocks: Calibration and application to tectonic exhumation in Crete, Greece. *Earth Planet. Sci. Lett.* 240, 339–354.

Rantitsch G., Grogger W., Teichert Ch., Ebner F., Hofer Ch., Maurer E.-M., Schaffer B. & Toth M. 2004: Conversion of carbonaceous material to graphite within the Greywacke Zone of the Eastern Alps. *Int. J. Earth Sci.* 93, 959–973.

Rantitsch G., Sachsenhofer R.F., Hasenhüttl Ch., Russegger B. & Rainer Th. 2005: Thermal evolution of an extensional detachment as constrained by organic metamorphic data and thermal modeling: Graz Paleozoic Nappe Complex (Eastern Alps). *Tectonophysics* 411, 57–72.

Ratschbacher L., Frisch W., Neubauer F., Schmid S.M. & Neugebauer J. 1989: Extension in compressional orogenic belts: the Eastern Alps. *Geology* 17, 404–407.

Ratschbacher L., Frisch W., Linzer H.G. & Merle O. 1991: Lateral extrusion in the Eastern Alps. Part II: Structural analysis. *Tectonics* 10, 257–271.

Ratschbacher L., Dingeldey C., Miller C., Hacke B.R. & Mc Williams M.O. 2004: Formation, subduction, and exhumation of Penninic oceanic crust in the Eastern Alps: Time constraints from $^{40}Ar/^{39}Ar$ geochronology. *Tectonophysics* 394, 155–170.

Reinecker J. & Lenhardt W.A. 1999: Present-day stress field and deformation in eastern Austria. *Int. J. Earth Sci.* 88, 532–550.

Robinson D. & Bevins R.E. 1986: Incipient metamorphism in the Lower Palaeozoic marginal basin of Wales. *J. Metamorph. Geology* 4, 101–113.

Robl J., Fritz H., Stüwe K. & Bernhard F. 2004: Cyclic fluid infiltration in structurally controlled Ag-Pb-Cu occurrences (Schladming, Eastern Alps). *Chem. Geol.* 205, 17–36.

Rosenberg C.L. & Schneider S. 2008: The western termination of the SEMP Fault (eastern Alps) and its bearing on the exhumation of the Tauern Window. *Geol. Soc. London, Spec. Publ.* 298, 197–218.

Sachsenhofer R.F. 1992: Coalification and thermal histories of Tertiary basins in relation to late Alpidic evolution of the Eastern Alps. *Geol. Rdsch.* 81, 291–308.

Sachsenhofer R.F. 2001: Syn- and post-collisional heat flow in the Tertiary Eastern Alps. *Int. J. Earth Sci.* 90, 579–592.

Sachsenhofer R.F., Rantitsch G., Hasenhüttl C., Jelen B. & Russegger B. 1998: Smectite-to-illite diagenesis in Early Miocene sediments from the hyperthermal Western Pannonian Basin. *Clay Miner.* 33, 523–537.

Sassi F.P. 1972: The petrological and geological significance of the b0 values of potassic white micas in low-grade metamorphic rocks. An application to Eastern Alps. *Tschermaks Mineral. Petrogr. Mitt.* 18, 105–113.

Sassi F.P. & Scolari A. 1974: The b0 value of the potassic white mica as a barometric indicator in low-grade metamorphism of pelitic schists. *Contr. Mineral. Petrology* 45, 143–152.

Schmid S.M., Fügenschuh B., Kissling E. & Schuster R. 2004: Tectonic map and overall architecture of the Alpine orogen. *Eclogae Geol. Helv.* 97, 93–117.

Schmidlechner M., Neubauer F. & Handler R. 2006: Extent and age of metamorphism of the central Grauwacken Zone, Eastern Alps: a $^{40}Ar/^{39}Ar$ study. *Pangeo Austria 2006 Abstracts*, Salzburg, 314–315.

Schramm J.-M. 1980: Bemerkungen zum Metamorphosegeschehen in klastischen Sedimentgesteinen im Salzburger Abschnitt der Grauwackenzone und der Nördlichen Kalkalpen. *Mitt. Österr. Geol. Gesell.* 71/72, 379–384.

Schramm J.-M. 1982: Überlegungen zur Metamorphose des klastischen Permoskyth der Nördlichen Kalkalpen vom Alpenostrand bis zum Rätikon (Österreich). *Verh. Geol. Bundesanst.* 1982, 73–83.

Schuster R., Koller F., Hoeck V., Hoinkes G. & Bousquet R. 2004: Explanatory notes to the map: Metamorphic structure of the Alps. Metamorphic evolution of the eastern Alps. *Mitt. Österr. Mineral. Gesell.* 149, 175–199.

Staufenberg H. 1987: Apatite fission-track evidence for postmetamorphic uplift and cooling history of the eastern Tauern window and the surrounding Austroalpine (central Eastern Alps, Austria). *Jb. Geol. Bundesanst.* 130, 571–586.

Tencer V. & Stüwe K. 2003: The metamorphic field gradient in the eclogite type locality, Koralpe region, Eastern Alps. *J. Metamorph. Geology* 21, 377–393.

Urbanek Ch. 2001: Transpressive und mehrphasige Deformation entlang der Salzachtalstörung am Nordrand des Tauernfensters (Österreich). *Diploma Thesis, Universität Wien*, 65 S.

Urbanek Ch., Frank W., Grasemann B. & Decker K. 2002: Eoalpine versus Tertiary deformation: Dating of heterogeneously partitioned strain (Tauern Window, Austria). *Pangeo Austria 2002, Proceedings*, 183–184.

Villa I.M. 1998: Isotope closure. *Terra Nova* 10, 42–47.

Wang X. & Neubauer F. 1998: Orogen-parallel strike-slip faults bordering metamorphic core complexes: the Salzach-Enns fault zone in the Eastern Alps, Austria. *J. Struct. Geol.* 20, 799–818.

Wiesinger M., Neubauer F. & Handler R. 2006: Exhumation of the Saualpe eclogite unit, Eastern Alps: constraints from $^{40}Ar/^{39}Ar$ ages and structural investigations. *Miner. Petrology* 88, 149–180.

Appendix

Sample localities (coordinates in the WGS84 coordinate system, formation names according to Heinisch et al. 1995, 2003).

Sample	N	E	Tectonic Unit		Locality	Formation	Lithology
50	47.42531	12.56854		Hochhörndler Imbricate Zone	Weissenstein Mine		Black slate
20	47.33041	12.72292			Schmittenhöhe		Black slate
21	47.33015	12.71022			Schmittenhöhe		Black slate
23	47.33195	12.70931			Schmittenhöhe		Slate
24	47.34452	12.70447			Schmittenhöhe		Lydite
25	47.33747	12.70358			Schmittenhöhe		Slate
26	47.32878	12.70028			Schmittenhöhe	Löhnersbach Fm	Slate
27	47.32151	12.74653			Breiteckalm		Siltstone
30	47.30883	12.76508			Areitalm		Slate
32	47.33168	12.62537	Greywacke Zone (Austroalpine Unit)	Glemmtal Unit	Klinglertörl	Klinger-Kar Fm	Black slate
33	47.33200	12.62536			Klinglertörl	Klinger-Kar Fm	Black slate
34	47.33199	12.62531			Klinglertörl	Klinger-Kar Fm	Lydite
35	47.33109	12.62507			Klinglertörl	Klinger-Kar Fm	Black slate
36	47.33195	12.62500			Klinglertörl	Klinger-Kar Fm	Black slate
37	47.33315	12.62389			Klinglertörl	Schattberg Fm	Siltstone
37a	47.33315	12.62389			Klinglertörl	Schattberg Fm	Siltstone
40	47.33559	12.62465			Klinglertörl	Klinger-Kar Fm	Black slate
41	47.36656	12.68918			Roseggraben		Slate
45	47.37757	13.00242			Dienten		Black slate
46	47.34420	13.01273			Sonnberg Dienten		Black slate
42	47.30124	12.68460		Uttendorfer Imbricate Zone	Walchen		Lydite
44	47.29535	12.58487			Uttendorf		Black slate
43	47.27032	12.61434	Penninic Unit	Glockner Nappe	Abendsberg	Bündnerschiefer	Calcareous slate